

Correlated atomic wires on substrates. I. Mapping to quasi-one-dimensional models

Anas Abdelwahab and Eric Jeckelmann

Leibniz Universität Hannover, Institut für Theoretische Physik, Appelstr. 2, 30167 Hannover, Germany

Martin Hohenadler

Institut für Theoretische Physik und Astrophysik, Universität Würzburg, Am Hubland, 97074 Würzburg, Germany

(Dated: March 10, 2022)

We present a theoretical study of correlated atomic wires deposited on substrates in two parts. In this first part, we propose lattice models for a one-dimensional quantum wire on a three-dimensional substrate and map them onto effective two-dimensional lattices using the Lanczos algorithm. We then discuss the approximation of these two-dimensional lattices by narrow ladder models that can be investigated with well-established methods for one-dimensional correlated quantum systems, such as the density-matrix renormalization group or bosonization. The validity of this approach is studied first for noninteracting electrons and then for a correlated wire with a Hubbard electron-electron repulsion using quantum Monte Carlo simulations. While narrow ladders cannot be used to represent wires on metallic substrates, they capture the physics of wires on insulating substrates if at least three legs are used. In the second part [arXiv:1704.07359], we use this approach for a detailed numerical investigation of a wire with a Hubbard-type interaction on an insulating substrate.

I. INTRODUCTION

The fascinating properties of one-dimensional (1D) electron systems have been studied theoretically for more than 60 years [1–6]. Experimentally, quasi-1D electron systems can now be realized in linear atomic wires deposited on a semiconducting substrate [7–9]. For instance, a Peierls metal-insulator transition occurs in indium chains on a Si(111) surface [9, 10], Luttinger liquid behavior is found in gold chains on Ge(100) [11] as well as in Bi chains on InSb(100) [12], and it is believed that linear chains of spin-polarized and localized electrons are formed at step edges of Si(hhk) surfaces [13]. Yet, the interpretation of experimental results often remains controversial. A fundamental issue is our poor theoretical understanding of the effects of the coupling between an atomic wire and its three-dimensional (3D) substrate on hallmark features of 1D systems such as the Peierls instability or Luttinger liquid behavior.

The theory of 1D electronic systems is mostly based on effective models for the low-energy degrees of freedom. The goal of this approach is to understand some generic physical phenomena within a simplified model rather than to achieve a full description of a specific material. Various quantum lattice models have become *de facto* standards for describing correlated electrons in quantum wires. One example is the 1D Hubbard model [5], which can describe several aspects of these systems such as Luttinger liquid physics, Mott-insulating behavior, and antiferromagnetic spin-density-wave correlations. Obviously, we must generalize these models to include the effects of the wire-substrate coupling.

As investigations of interacting electrons on 3D lattices with complex geometries are extremely difficult, the modeling of wire-substrate systems by much simpler effective models appears to be a very promising route. Asymmetric two-leg ladder systems provide a minimal model for such systems [7, 14–16]. One leg

represents the atomic wire, while the second leg mimics those degrees of freedom of the substrate that couple to the wire. For instance, this approach was used to study the stability of Luttinger liquids [14, 15] and Peierls insulators [7] coupled to an environment. The main advantage of these ladder models is that one can study them with well-established methods for 1D correlated systems such as the numerical density-matrix renormalization group (DMRG) [17–20] or field-theoretical techniques (e.g., bosonization and the renormalization group) [1, 6, 21–23]. A significant drawback is that a single leg may be insufficient to represent the role of the 3D substrate [16]. Until now, this approach has not been pursued systematically.

In this paper, we show how to systematically construct effective quasi-1D ladder models for wire-substrate systems. Our method generalizes an approach recently proposed to map multi-orbital, multi-site quantum impurity problems onto ladder systems [24, 25]. We show that if the wire-substrate system is translationally invariant in the wire direction, it can be mapped exactly onto a wide ladder-like lattice [i.e., an anisotropic (semi-infinite) two-dimensional (2D) lattice]. This mapping is illustrated in Fig. 1. The key idea is to decompose the full system into independent single-impurity systems using the momentum-space representation in the wire direction, then to perform the usual transformation of each impurity system into a long chain [26, 27], which finally becomes one rung of a wide ladder after transforming back to real space in the wire direction. The main difference between Refs. [24, 25] and our method is that in the former the number of impurity sites and orbitals determines the ladder width and the number of single-particle host states sets the ladder length. In contrast, in our approach, the wire length determines the ladder length and the number of single-particle substrate states sets the ladder width.

If the number of ladder legs (i.e., the number of shells

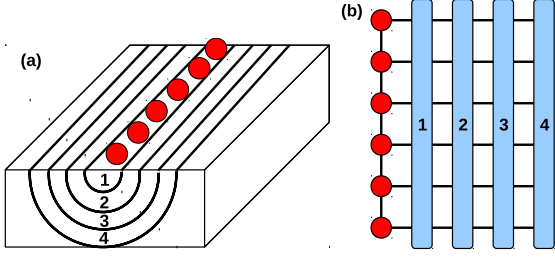


FIG. 1. (Color online) (a) Sketch of an atomic wire (red spheres) on a 3D substrate with four numbered shells. (b) Ladder representation of the same system with the left-most leg corresponding to the atomic wire (red circles) and the other legs (in blue) representing shells one to four.

in the substrate) is small, we obtain a quasi-1D problem that can be treated efficiently by methods for 1D correlated electron systems. Thus, we investigate the approximation of the full wire-substrate system in its ladder representation by narrow effective ladders. We find the approximation to be valid for an insulating substrate if at least three legs are kept, but never for a metallic substrate. To illustrate our procedure, we introduce an electronic 3D lattice model describing an interacting wire on a noninteracting substrate. The procedure is demonstrated explicitly first for a noninteracting wire and then for a correlated Hubbard wire using quantum Monte Carlo (QMC) simulations [28, 29]. In [30], we use DMRG and QMC methods to investigate in detail the case of a wire with a Hubbard-type interaction on an insulating substrate.

This paper is structured as follows. In Sec. II, we introduce 3D lattice models for wire-substrate systems. The exact mapping of these models onto wide ladders is presented in Sec. III. In Sec. IV, we discuss their approximation by effective narrow ladders. Finally, Sec. V contains our conclusions.

II. WIRE-SUBSTRATE MODEL

In this section, we introduce a model for a single correlated wire on the surface of a noninteracting 3D substrate, which we will use in Sec. III to illustrate the mapping to ladder systems. Interactions with other wires are assumed to be negligible for the low-energy physics. While this is not justified for phases with long-range order, such as Peierls, spin-density-wave, and charge-density-wave states, it is a reasonable approximation for Luttinger liquid phases or paramagnetic Mott insulators, which are our main concern here. The system Hamiltonian can be decomposed into three terms,

$$H = H_s + H_w + H_{ws}, \quad (1)$$

where H_s describes the substrate degrees of freedom, H_w the wire degrees of freedom, and H_{ws} the coupling between wire and substrate. Although the present approach

can be applied to models that also include lattice degrees of freedom (phonons), we focus on purely electronic models and discuss possible extensions at the end of this section. We set $\hbar = 1$ and do not distinguish between momentum and wave number.

A. Substrate

The substrate is represented by a cubic lattice with lattice constants $a = b = c = 1$. The coordinate axes are set by the lattice primitive vectors. Thus the lattice sites have positions $\mathbf{r} = (x, y, z)$ with $x, y, z \in \mathbb{Z}$. The substrate extends over L_x, L_y and L_z sites in the x, y and z -directions, respectively. We use periodic boundary conditions in the x and y -directions but open boundary conditions in the z -direction. The substrate surface lies in the xy -plane and the surface layer corresponds to $z = 1$. Thus, objects on the surface have a coordinate $z = 0$.

We first introduce the simpler Hamiltonian for a metallic substrate and then generalize it to case of an insulating substrate. (There is at least a theoretical interest in 1D atomic structures on metallic substrates [31].) A simple model for the electronic degrees of freedom of a metallic substrate is given by a tight-binding Hamiltonian with onsite potential ϵ_s and nearest-neighbor hopping t_s ,

$$H_s = \epsilon_s \sum_{\mathbf{r}, \sigma} n_{s\mathbf{r}\sigma} - t_s \sum_{\langle \mathbf{r}\mathbf{q} \rangle} \sum_{\sigma} (c_{s\mathbf{r}\sigma}^\dagger c_{s\mathbf{q}\sigma} + \text{H.c.}). \quad (2)$$

The first sum runs over all lattice sites and the second one over all pairs $\langle \mathbf{r}\mathbf{q} \rangle$ of nearest-neighbor sites. The operator $c_{s\mathbf{r}\sigma}^\dagger$ creates an electron with spin σ on the site with coordinates $\mathbf{r} = (x, y, z)$, and the density operator for electrons with spin σ is $n_{s\mathbf{r}\sigma} = c_{s\mathbf{r}\sigma}^\dagger c_{s\mathbf{r}\sigma}$. Hamiltonian (2) can be diagonalized by the usual canonical transformation to momentum space,

$$d_{s\mathbf{k}\sigma}^\dagger = \sum_{\mathbf{r}} \psi_{\mathbf{k}}(\mathbf{r}) c_{s\mathbf{r}\sigma}^\dagger, \quad (3)$$

with the single-particle eigenstates

$$\psi_{\mathbf{k}}(\mathbf{r}) = \frac{1}{\sqrt{L_x}} e^{ik_x x} \frac{1}{\sqrt{L_y}} e^{ik_y y} \sqrt{\frac{2}{L_z + 1}} \sin(k_z z). \quad (4)$$

The inverse transformation is then given by

$$c_{s\mathbf{r}\sigma}^\dagger = \sum_{\mathbf{k}} \psi_{\mathbf{k}}^*(\mathbf{r}) d_{s\mathbf{k}\sigma}^\dagger, \quad (5)$$

where the sum is over all sites \mathbf{k} of the reciprocal lattice. Here, $\mathbf{k} = (k_x, k_y, k_z)$ with

$$k_x = \frac{2\pi}{L_x} n_x, \quad n_x \in \mathbb{Z}, \quad -\frac{L_x}{2} < n_x \leq \frac{L_x}{2}, \quad (6a)$$

$$k_y = \frac{2\pi}{L_y} n_y, \quad n_y \in \mathbb{Z}, \quad -\frac{L_y}{2} < n_y \leq \frac{L_y}{2}, \quad (6b)$$

$$k_z = \frac{\pi}{L_z + 1} n_z, \quad n_z \in \mathbb{Z}, \quad 1 \leq n_z \leq L_z. \quad (6c)$$

The differences between the z -component and the other two components in Eqs. (4) and (6) reflect the different boundary conditions. In the momentum-space representation Hamiltonian (2) becomes diagonal,

$$H_s = \sum_{\mathbf{k}, \sigma} \epsilon_s(\mathbf{k}) d_{s\mathbf{k}\sigma}^\dagger d_{s\mathbf{k}\sigma}, \quad (7)$$

with a single-electron dispersion

$$\epsilon_s(\mathbf{k}) = \epsilon_s - 2t_s[\cos(k_x) + \cos(k_y) + \cos(k_z)]. \quad (8)$$

In reality, most substrates for atomic wires are not metallic but insulating or semiconducting [7–9]. A simple model for an insulating substrate consists of a valence band and a conduction band separated by a gap. It can be constructed using the same lattice as above but with two orbitals per site with different onsite energies ϵ_v and ϵ_c . The Hamiltonian then takes the form

$$H_s = H_v + H_c, \quad (9)$$

where the valence-band Hamiltonian

$$H_v = \epsilon_v \sum_{\mathbf{r}, \sigma} n_{v\mathbf{r}\sigma} - t_v \sum_{\langle \mathbf{r}\mathbf{q} \rangle} \sum_{\sigma} (c_{v\mathbf{r}\sigma}^\dagger c_{v\mathbf{q}\sigma} + \text{H.c.}) \quad (10)$$

and the conduction-band Hamiltonian

$$H_c = \epsilon_c \sum_{\mathbf{r}, \sigma} n_{c\mathbf{r}\sigma} - t_c \sum_{\langle \mathbf{r}\mathbf{q} \rangle} \sum_{\sigma} (c_{c\mathbf{r}\sigma}^\dagger c_{c\mathbf{q}\sigma} + \text{H.c.}) \quad (11)$$

are tight-binding Hamiltonians with nearest-neighbor hopping terms t_v and t_c , respectively. Accordingly, $c_{v\mathbf{r}\sigma}^\dagger$ and $c_{c\mathbf{r}\sigma}^\dagger$ create electrons with spin σ on site \mathbf{r} in the localized orbitals corresponding to the valence and conduction bands, while $n_{v\mathbf{r}\sigma}$ and $n_{c\mathbf{r}\sigma}$ denote the corresponding density operators. The canonical transformation from real to momentum space (3) can be generalized to diagonalize these Hamiltonians. This leads to

$$H_v = \sum_{\mathbf{k}, \sigma} \epsilon_v(\mathbf{k}) d_{v\mathbf{k}\sigma}^\dagger d_{v\mathbf{k}\sigma} \quad (12)$$

and

$$H_c = \sum_{\mathbf{k}, \sigma} \epsilon_c(\mathbf{k}) d_{c\mathbf{k}\sigma}^\dagger d_{c\mathbf{k}\sigma} \quad (13)$$

with single-electron dispersions $\epsilon_v(\mathbf{k})$ and $\epsilon_c(\mathbf{k})$ of the form (8) but with $\{\epsilon_s, t_s\}$ replaced by $\{\epsilon_v, t_v\}$ and $\{\epsilon_c, t_c\}$, respectively. The (possibly indirect) gap between the bottom of the conduction band and the top of the valence band is $\Delta_s = \epsilon_c - \epsilon_v - 6(|t_v| + |t_c|)$ and the condition $\Delta_s \geq 0$ restricts the range of allowed model parameters.

B. Wire

The atomic wire is represented by a 1D chain aligned with the x -direction on the substrate surface. To simplify

the problem as much as possible, we assume that the wire extends over the full length of the substrate, that the lattice constants of wire and substrate are equal, and that every site of the wire lies exactly above the corresponding substrate site. Thus the L_x wire sites have positions $\mathbf{r} = (x, y_0, 0)$ with $x = 1, \dots, L_x$ and a fixed $y_0 \in \{1, \dots, L_y\}$.

The 1D Hubbard model [5] describes the effects of electronic correlations on the low-energy properties of 1D lattice systems. It is integrable and has been solved using the Bethe ansatz method. Its ground state for repulsive interactions is a Mott insulator at half-filling but a paramagnetic 1D metal with the low-energy properties of a Luttinger liquid away from half-filling [6]. Here, we use it to model the atomic wire. The Hamiltonian is

$$H_w = \epsilon_w \sum_{x, \sigma} n_{wx\sigma} - t_w \sum_{x, \sigma} (c_{wx\sigma}^\dagger c_{w, x+1, \sigma} + \text{H.c.}) + U \sum_x n_{wx\uparrow} n_{wx\downarrow}, \quad (14)$$

where x runs over all wire sites, $c_{wx\sigma}^\dagger$ creates an electron with spin σ on the wire site at $\mathbf{r} = (x, y_0, 0)$, and the density operator for electrons with spin σ is $n_{wx\sigma} = c_{wx\sigma}^\dagger c_{wx\sigma}$. The Hubbard term of strength U describes the repulsion between two electrons on the same site, t_w is the usual hopping term between nearest-neighbor sites, and ϵ_w is the onsite potential.

The momentum-space representation of Eq. (14) is

$$H_w = \sum_{k, \sigma} \epsilon_w(k) d_{wk\sigma}^\dagger d_{wk\sigma} + \frac{U}{L_x} \sum_{k, p, k', p'} d_{wk\uparrow}^\dagger d_{wp\uparrow} d_{wk'\downarrow}^\dagger d_{wp'\downarrow} \delta_{k-p, p'-k'} \quad (15)$$

with the single-electron dispersion

$$\epsilon_w(k) = \epsilon_w - 2t_w \cos(k). \quad (16)$$

The canonical transformation between real and momentum space is given by

$$d_{wk\sigma}^\dagger = \frac{1}{\sqrt{L_x}} \sum_x e^{ikx} c_{wx\sigma}^\dagger. \quad (17)$$

The operator $d_{wk\sigma}^\dagger$ creates an electron with spin σ in an orbital with momentum k in the x -direction and at position $(y_0, 0)$ in the yz -plane. In the above equations the indices k, p, k' , and p' denote momenta in the x -direction, see Eq. (6a). It is important to understand that in the framework of the 3D wire-substrate model the above form of the Hubbard Hamiltonian corresponds to a mixed real-space/momentum-space representation.

C. Wire-substrate hybridization

The simplest coupling between the wire and the substrate consists of a hybridization of the electronic orbitals. This can be realized with a hopping term between

nearest-neighbor pairs of sites located in the wire and the substrate, respectively.

For a metallic substrate we define

$$H_{ws} = -t_{ws} \sum_{x,\sigma} (c_{s\mathbf{r}\sigma}^\dagger c_{w\mathbf{x}\sigma} + \text{H.c.}) \quad (18)$$

with $\mathbf{r} = (x, y_0, 1)$. In the momentum-space representation this yields

$$H_{ws} = \sum_{\mathbf{k}\sigma} \left[\Gamma_{ws}(\mathbf{k}) d_{s\mathbf{k}\sigma}^\dagger d_{w\mathbf{k}_x\sigma} + \text{H.c.} \right] \quad (19)$$

with a k_x -independent hybridization function

$$\Gamma_{ws}(\mathbf{k}) = -t_{ws} \sqrt{\frac{2}{L_y(L_z + 1)}} \exp(-ik_y y_0) \sin(k_z). \quad (20)$$

For an insulating substrate with two orbitals per site the hybridization strengths can be different for the valence and conduction bands, and we define

$$H_{ws} = H_{wv} + H_{wc} \quad (21)$$

with the hybridization between wire and valence band

$$H_{wv} = -t_{wv} \sum_{x,\sigma} (c_{v\mathbf{r}\sigma}^\dagger c_{w\mathbf{x}\sigma} + \text{H.c.}) \quad (22)$$

and the hybridization between wire and conduction band

$$H_{wc} = -t_{wc} \sum_{x,\sigma} (c_{c\mathbf{r}\sigma}^\dagger c_{w\mathbf{x}\sigma} + \text{H.c.}). \quad (23)$$

In the momentum-space representation, H_{wv} and H_{wc} are given by expressions similar to Eq. (19),

$$H_{wv} = \sum_{\mathbf{k}\sigma} \left[\Gamma_{wv}(\mathbf{k}) d_{v\mathbf{k}\sigma}^\dagger d_{w\mathbf{k}_x\sigma} + \text{H.c.} \right], \quad (24)$$

$$H_{wc} = \sum_{\mathbf{k}\sigma} \left[\Gamma_{wc}(\mathbf{k}) d_{c\mathbf{k}\sigma}^\dagger d_{w\mathbf{k}_x\sigma} + \text{H.c.} \right], \quad (25)$$

with $\Gamma_{wv}(\mathbf{k})$ and $\Gamma_{wc}(\mathbf{k})$ identical to Eq. (20) except for the replacement of t_{ws} by t_{wv} and t_{wc} , respectively.

D. Generalizations

Our wire-substrate model may be extended in several ways. For instance, the substrate properties and the wire-substrate coupling can be changed without difficulty in the momentum-space representation. For the substrate band structure we can consider general single-particle dispersions $\epsilon_b(\mathbf{k})$ ($b = s, v, c$) beyond the simple cosine form (8). For the wire-substrate coupling we can define hybridization functions $\Gamma_{wb}(\mathbf{k})$ ($b = s, v, c$) with a more general \mathbf{k} dependence than in Eq. (20). Other possible

generalizations are the modification of the wire dispersion (16), or the inclusion of inter-site electron-electron interactions in the wire Hamiltonian (14).

Even more complicated generalizations include multiple electronic bands for the substrate or the wire and changes of the lattice geometry or the unit cell. Furthermore, we can also include phonon degrees of freedom in the model, with an electron-phonon coupling in the wire and a hybridization of wire and substrate phonon modes.

III. EXACT LADDER REPRESENTATION

In this section, we explain how the wire-substrate system can be mapped onto a wide ladder or anisotropic 2D lattice. First, the system is cut into slices perpendicular to the wire direction in momentum space to obtain independent impurity problems with 2D hosts. In a second step, the impurity problems are mapped onto 1D chains. Finally, the full system is transformed back to a ladder lattice in real space.

A. Impurity subsystems

We first analyze Hamiltonian (1) for a noninteracting wire ($U = 0$). In momentum space, it can be written as a sum of independent terms,

$$H = \sum_{k_x, \sigma} H_{k_x \sigma}, \quad (26)$$

with

$$H_{k_x \sigma} = \epsilon_w(k_x) d_{wk_x \sigma}^\dagger d_{wk_x \sigma} + \sum_{k_y, k_z} \epsilon_s(\mathbf{k}) d_{s\mathbf{k}\sigma}^\dagger d_{s\mathbf{k}\sigma} + \sum_{k_y, k_z} \left[\Gamma_{ws}(\mathbf{k}) d_{s\mathbf{k}\sigma}^\dagger d_{wk_x \sigma} + \text{H.c.} \right] \quad (27)$$

for a metallic substrate, or

$$H_{k_x \sigma} = \epsilon_w(k_x) d_{wk_x \sigma}^\dagger d_{wk_x \sigma} + \sum_{k_y, k_z} \epsilon_c(\mathbf{k}) d_{c\mathbf{k}\sigma}^\dagger d_{c\mathbf{k}\sigma} + \sum_{k_y, k_z} \epsilon_v(\mathbf{k}) d_{v\mathbf{k}\sigma}^\dagger d_{v\mathbf{k}\sigma} + \sum_{k_y, k_z} \left[\Gamma_{wc}(\mathbf{k}) d_{c\mathbf{k}\sigma}^\dagger d_{wk_x \sigma} + \text{H.c.} \right] + \sum_{k_y, k_z} \left[\Gamma_{wv}(\mathbf{k}) d_{v\mathbf{k}\sigma}^\dagger d_{wk_x \sigma} + \text{H.c.} \right] \quad (28)$$

for an insulating substrate.

In either case we have $[H_{k_x \sigma}, H_{k'_x \sigma'}] = 0 \ \forall k_x, k'_x, \sigma, \sigma'$. Therefore, each Hamiltonian $H_{k_x \sigma}$ can be diagonalized and discussed separately. In the absence of electron-electron interactions, it corresponds to a single-particle Hamiltonian acting on N_{imp} sites, with $N_{\text{imp}} = L_y L_z + 1$ for a metallic substrate and $N_{\text{imp}} = 2L_y L_z + 1$ for an insulating substrate. Each $H_{k_x \sigma}$ describes a nonmagnetic

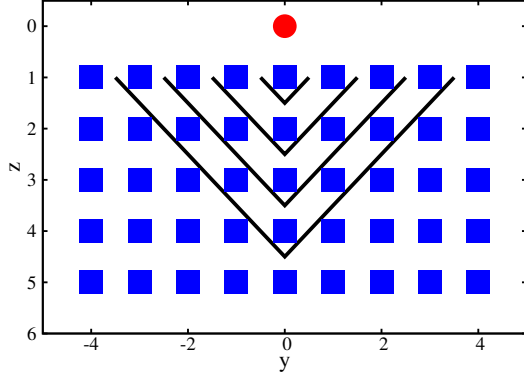


FIG. 2. (Color online) Sketch of the impurity subsystem in the mixed representation with $L_y = 9$ and $L_z = 5$. The wire site (impurity) is represented by the red circle at $(y_0 = 0, z = 0)$ while the substrate sites (host) correspond to the blue squares. Black lines indicate the first, second, third, and fourth shells (from top to bottom) around the impurity.

impurity (the wire site with momentum k_x) coupled to a two-dimensional homogeneous host [the (k_y, k_z) -slice of the substrate for a given k_x]. The impurity energy level is $\epsilon_w(k_x)$. For a given k_x the host energies lie in a band between the minimum and maximum of $\epsilon_s(\mathbf{k})$ for a metallic substrate, and in a band between the extrema of $\epsilon_c(\mathbf{k})$ and $\epsilon_v(\mathbf{k})$ for an insulating substrate. For each k_x the coupling between impurity and host is described by the hybridization functions $\Gamma_{wb}(\mathbf{k})$.

The Hamiltonian H can also be written in a mixed representation combining momentum space in one direction (k_x) and real space in the other two directions (y, z). In this representation, each $H_{k_x\sigma}$ acts on a (y, z) -slice of the wire-substrate system for the given wave vector in the x -direction, as illustrated in Fig. 2.

If the substrate slice (host) is infinitely large ($N_{\text{imp}} \rightarrow \infty$), the single-particle eigenenergies of each $H_{k_x\sigma}$ form one (metallic substrate) or two (insulating substrate) continua. It is well known [32] that an eigenenergy either lies in a continuum and the corresponding eigenstate is delocalized in the impurity-host system, or the eigenenergy lies outside any continuum and the eigenstate is localized around the impurity. In the 3D wire-substrate system the former case corresponds to states delocalized in the substrate while the latter corresponds to states localized in or around the wire.

B. Chain representation

Each impurity Hamiltonian $H_{k_x\sigma}$ can be mapped onto a 1D tight-binding chain with diagonal terms and nearest-neighbor hoppings only using the usual procedure [26, 27] based on the Lanczos tridiagonalization algorithm. The procedure is initialized with the single-electron states $|k_x, -1, \sigma\rangle = 0$ and $|k_x, 0, \sigma\rangle = d_{wk_x\sigma}^\dagger |\emptyset\rangle$, where $|\emptyset\rangle$ is the vacuum state. The orthogonal one-

particle states $|k_x, n, \sigma\rangle$ for $n = 1, \dots, N_{\text{imp}} - 1$ are then generated iteratively using

$$|k_x, n+1, \sigma\rangle = H_{k_x\sigma} |k_x, n, \sigma\rangle - A_n(k_x) |k_x, n, \sigma\rangle - B_n^2(k_x) |k_x, n-1, \sigma\rangle, \quad (29)$$

where the coefficients are given by

$$A_n(k_x) = \frac{\langle k_x, n, \sigma | H_{k_x\sigma} | k_x, n, \sigma \rangle}{\langle k_x, n, \sigma | k_x, n, \sigma \rangle} \quad (30)$$

for $n = 0, \dots, N_{\text{imp}} - 1$ and by

$$B_n^2(k_x) = \frac{\langle k_x, n, \sigma | k_x, n, \sigma \rangle}{\langle k_x, n-1, \sigma | k_x, n-1, \sigma \rangle} \quad (31)$$

for $n = 1, \dots, N_{\text{imp}} - 1$ with $B_0(k_x) = 0$. In the Lanczos (or chain) representation, the Hamiltonian takes the form

$$H_{k_x\sigma} = \sum_{n=0}^{N_{\text{imp}}-1} A_n(k_x) f_{k_x n \sigma}^\dagger f_{k_x n \sigma} + \sum_{n=0}^{N_{\text{imp}}-2} \left[B_{n+1}(k_x) f_{k_x n \sigma}^\dagger f_{k_x, n+1, \sigma} + \text{H.c.} \right], \quad (32)$$

where the new fermion operators $f_{k_x n \sigma}^\dagger$ create electrons in the states $|k_x, n, \sigma\rangle$. Since the wire-substrate model is invariant under spin rotation, the transformation from the old to the new fermion operators as well as the coefficients A_n and B_n do not depend on spin.

This canonical transformation can be carried out numerically even when N_{imp} is as large as 10^4 . We note that the wire states are not modified by the transformation, i.e., $f_{k_x, n=0, \sigma}^\dagger = d_{wk_x\sigma}^\dagger$. Moreover, one can easily show that $A_0(k_x) = \epsilon_w(k_x)$ and

$$B_1^2(k_x) = \sum_{k_y, k_z} |\Gamma_{ws}(\mathbf{k})|^2 \quad (33)$$

for the metallic substrate, while

$$B_1^2(k_x) = \sum_{k_y, k_z} [|\Gamma_{wc}(\mathbf{k})|^2 + |\Gamma_{wv}(\mathbf{k})|^2] \quad (34)$$

for the insulating substrate.

If we take the dispersion (8) and the hybridization (20) for the metallic substrate, the impurity system is relatively simple in the mixed representation of Fig. 2. The impurity onsite potential is $\epsilon_w(k_x)$ while it is $\epsilon_s - t_s \cos(k_x)$ for the host sites. A hopping t_{ws} between the impurity and the nearest host site is the only coupling between impurity and host. Moreover, the host sites are coupled by nearest-neighbor hopping terms t_s . The state $|k_x, n, \sigma\rangle$ is entirely localized in a shell including the host sites that are m -th nearest neighbors of the impurity with $m \leq n$. These shells are shown in Fig. 2. In addition, we can show that $A_n(k_x) = \epsilon_s - 2t_s \cos(k_x)$ for $n \geq 1$.

The first few off-diagonal coefficients can be computed analytically:

$$B_1^2(k_x) = t_{\text{ws}}^2, \quad (35a)$$

$$B_2^2(k_x) = 3t_s^2, \quad (35b)$$

$$B_3^2(k_x) = \frac{11}{3}t_s^2, \quad (35c)$$

$$B_4^2(k_x) = \frac{125}{33}t_s^2. \quad (35d)$$

Similarly, we obtain for the insulating substrate

$$A_1(k_x) = \frac{t_{\text{wc}}^2 [\epsilon_c - 2t_c \cos(k_x)] + t_{\text{wv}}^2 [\epsilon_v - 2t_v \cos(k_x)]}{t_{\text{wc}}^2 + t_{\text{wv}}^2}$$

and

$$B_1^2(k_x) = \Gamma^2(k_x) = t_{\text{wc}}^2 + t_{\text{wv}}^2.$$

If we assume that the valence and conduction bands are similar, i.e., $t_v = t_c = t_s$ and $t_{\text{wc}}^2 = t_{\text{wv}}^2 = t_{\text{ws}}^2$, we can show that $A_n(k_x) = \frac{\epsilon_c + \epsilon_v}{2} - 2t_s \cos(k_x)$ for $n \geq 1$ and

$$B_1^2(k_x) = 2t_{\text{ws}}^2, \quad (36a)$$

$$B_2^2(k_x) = 3t_s^2 + \left(\frac{\epsilon_c - \epsilon_v}{2} \right)^2. \quad (36b)$$

C. Real-space representation

The full Hamiltonian (1) can now be written using Eq. (26) and the chain representations of $H_{k_x\sigma}$, then transformed back into the real-space representation in the x -direction. As the wire states have not been modified by the mapping of the impurity subsystem to the chain representation, the wire Hamiltonian H_w remains unchanged. The hybridization Hamiltonian becomes

$$H_{\text{ws}} = \sum_{x,x',\sigma} \left[\Gamma(x-x') g_{x,n=1,\sigma}^\dagger c_{wx'\sigma} + \text{H.c.} \right] \quad (37)$$

where we defined new fermion operators

$$g_{xn\sigma}^\dagger = \frac{1}{\sqrt{L_x}} \sum_{k_x} e^{-ik_x x} f_{k_x n \sigma}^\dagger \quad (38)$$

that create electrons with spin σ at position x in the n -th shell, and with the hopping amplitudes

$$\Gamma(x) = \frac{1}{L_x} \sum_q B_1(k_x) \exp(ik_x x) \quad (39)$$

between wire sites and sites in the first shell in the substrate. The substrate Hamiltonian becomes

$$H = \sum_{n=1}^{N_{\text{imp}}-1} \sum_{xx'\sigma} A_n(x-x') g_{xn\sigma}^\dagger g_{x'n\sigma} + \sum_{n=1}^{N_{\text{imp}}-2} \sum_{xx'\sigma} \left[B_{n+1}(x-x') g_{xn\sigma}^\dagger g_{x',n+1,\sigma} + \text{H.c.} \right] \quad (40)$$

with the hopping amplitudes

$$A_n(x) = \frac{1}{L_x} \sum_{k_x} A_n(k_x) \exp(ik_x x) \quad (41)$$

in the wire direction within the same shell n (or the onsite potential for $x = 0$) and the hopping amplitudes

$$B_{n+1}(x) = \frac{1}{L_x} \sum_{k_x} B_{n+1}(k_x) \exp(ik_x x) \quad (42)$$

between sites in shells n and $n+1$. Therefore, we have obtained a new representation of the Hamiltonian H with long-range hoppings on a 2D lattice of size $L_x \times N_{\text{imp}}$.

This complex system can be simplified considerably if we assume that the hybridization functions are independent of the x -component of the wave vector \mathbf{k} ,

$$\Gamma_{\text{wb}}(\mathbf{k}) = \Gamma_{\text{wb}}(k_y, k_z) \quad (\text{b=s,c,v}) \quad (43)$$

and that the dispersions have the additive form

$$\epsilon_b(\mathbf{k}) = \nu(k_x) + \epsilon_b(k_y, k_z) \quad (\text{b=s,c,v}). \quad (44)$$

[These conditions are fulfilled for the tight-binding Hamiltonians defined in Sec. II, see, e.g., Eqs. (8) and (20), but $t_c = t_v = t_s$ is required for the insulating substrate.] In that case, the impurity Hamiltonians $H_{k_x\sigma}$ depend on the momentum k_x only through the impurity onsite potential $\epsilon_w(k_x)$ and a constant energy shift $\nu(k_x)$ in the substrate. Therefore, the chain representations of the substrate are identical for all wave vectors k_x up to energy shifts. It follows that the hybridization between wire and substrate is

$$\Gamma(x) = \Gamma \delta_{x,0} \quad (45)$$

with $\Gamma = B_1(k_x)$ and that the hopping terms between nearest-neighbor shells are

$$B_n(x) = -t_n^{\text{rung}} \delta_{x,0} \quad (n \geq 2) \quad (46)$$

with $t_n^{\text{rung}} = -B_n(k_x)$. In addition, one finds that

$$A_n(x) = -t_x^{\text{leg}} + \mu_n \delta_{x,0} \quad (n \geq 1) \quad (47)$$

with

$$t_x^{\text{leg}} = -\frac{1}{L_x} \sum_{k_x} \nu(k_x) \exp(ik_x x) \quad (48)$$

and $\mu_n = A_n(k_x) - \nu(k_x)$.

At this point, we have obtained a representation of the wire-substrate Hamiltonian H in the form of ladder system with L_x rungs and N_{imp} legs, as sketched in Fig. 1. The leg with $n = 0$ is the wire, in particular $g_{x,n=0,\sigma}^\dagger = c_{wx\sigma}^\dagger$, while legs with $n = 1, \dots, N_{\text{imp}} - 1$ correspond to the successive shells and represent the substrate. The full Hamiltonian (1) consists of the unchanged wire Hamiltonian H_w , a hopping term Γ (hybridization) between sites at the same position x in the

wire and the first leg, a nearest-neighbor rung hopping t_n^{rung} between substrate legs $n-1$ and n , an onsite potential $\mu_n - t_0^{\text{leg}}$ constant within each substrate leg, and the same intra-leg hopping terms t_x^{leg} in every substrate leg; the latter are identical to the hopping terms in the original substrate Hamiltonian H_s .

Equations (43) and (44) are the main conditions on the wire-substrate system to make the mapping possible, in addition to translation symmetry in the x -direction. Although we have derived the mapping for a noninteracting wire only, it is clear that the wire sites and their Hamiltonian H_w are not modified by the transformation of the substrate. Therefore, the mapping remains valid even if H_w includes a Hubbard repulsion, more general electron-electron interactions, or electron-phonon coupling.

For substrates with dispersions of the form (8) we have $\nu(k_x) = -2t_s \cos(k_x)$, so that hopping within substrate legs takes place between nearest-neighbors only,

$$t_x^{\text{leg}} = \begin{cases} t_s & \text{if } |x| = 1, \\ 0 & \text{otherwise.} \end{cases} \quad (49)$$

The explicit form of the full Hamiltonian is then

$$\begin{aligned} H = & H_w + \sum_{x,\sigma} \left(\Gamma g_{x,n=1,\sigma}^\dagger c_{wx\sigma} + \text{H.c.} \right) \\ & + \sum_{n=1}^{N_{\text{imp}}-1} \sum_{x,\sigma} \mu_n g_{xn\sigma}^\dagger g_{xn\sigma} \\ & - t_s \sum_{n=1}^{N_{\text{imp}}-1} \sum_{x,\sigma} \left(g_{xn\sigma}^\dagger g_{x+1,n\sigma} + \text{H.c.} \right) \\ & - \sum_{n=1}^{N_{\text{imp}}-2} \sum_{x,\sigma} \left(t_{n+1}^{\text{rung}} g_{xn\sigma}^\dagger g_{x,n+1,\sigma} + \text{H.c.} \right). \end{aligned} \quad (50)$$

For the metallic substrate, $\mu_n = \epsilon_s$, $\Gamma = -t_{ws}$, and the first few hoppings $t_n^{\text{rung}} = -B_n(k_x)$ are given by Eq. (35). For the insulating substrate with $t_c = t_v = t_s$ and $t_{wc}^2 = t_{wv}^2 = t_{ws}^2$, we have $\mu_n = (\epsilon_c + \epsilon_v)/2$, $\Gamma = -B_1(k_x)$, and $t_2^{\text{rung}} = -B_2(k_x)$ as given by Eq. (36). The hopping terms t_n^{rung} for larger n can be computed numerically with the Lanczos algorithm, as described in Sec. III B. Figure 3 shows the hopping terms calculated for a metallic and an insulating substrate. We see that for large n they converge to about $2t_s$ in the metallic case. The feature near $n = 32$ is due to the finite substrate size used in the calculation ($L_y = 32$ and $L_z = 16$). In the insulating case, the hopping terms oscillate between $3t_s$ and about $7t_s$, as required to generate the gap $\approx \epsilon_c - \epsilon_v$ between valence and conduction bands at a fixed k_x in this representation of the substrate. Equation (36) shows the different dependence of the first two hopping terms on $\epsilon_c - \epsilon_v$ explicitly.

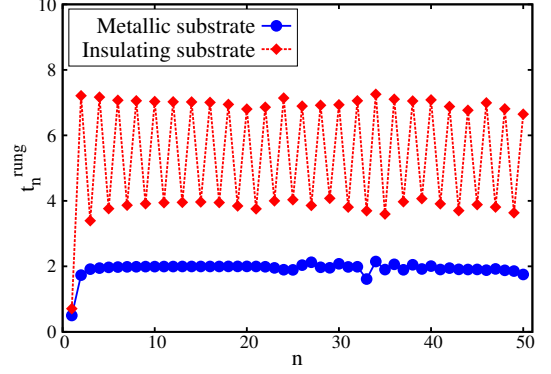


FIG. 3. (Color online) Hopping integrals t_n^{rung} between legs $n-1$ and n calculated numerically with the Lanczos algorithm for a metallic substrate (circles, $t_s = 1$, $t_{ws}^2 = 0.25$, $L_y = 32$, $L_z = 16$) and an insulating substrate (diamonds, $t_c = t_v = 1$, $t_{wc}^2 = t_{wv}^2 = 0.25$, $\epsilon_c = -\epsilon_v = 7$, $L_y = 32$, $L_z = 8$).

D. Alternative representations

The condition (44) is inconvenient for the insulating substrate because it imposes the same dispersion $\nu(k_x)$ in the k_x -direction in the valence and conduction bands to obtain a ladder-like Hamiltonian. However, it is possible to overcome this restriction by using an alternative mapping. Since the electronic states of the conduction and valence bands interact only through the impurity site, we can use a two-chain representation of the impurity problem where one chain represents the valence-band sites and the other the conduction-band sites. (A similar two-chain representation is used for the lower and upper Hubbard bands in Mott-Hubbard insulators [33].) Each chain can be generated separately using the Lanczos algorithm as described in Sec. III B. This yields a ladder-like Hamiltonian if condition (44) is satisfied separately by the conduction and valence bands, i.e., the dispersions $\nu_c(k_x)$ and $\nu_v(k_x)$ can be different. The wire is then the middle leg of the ladder and the legs representing valence and conduction bands extend on either side. The Hamiltonian parameters $A_n(k_x)$, and $B_n(k_x)$ are given by equations similar to those obtained for the metallic substrate, e.g., by Eq. (35) with $\{\epsilon_s, t_s\}$ replaced by $\{\epsilon_v, t_v\}$ and $\{\epsilon_c, t_c\}$, respectively.

The condition of a translationally invariant wire may be relaxed by performing the mapping first for a substrate decoupled from the wire and then connecting the two subsystems via the hybridization term. Such a generalization allows us to consider wires with disorder, a periodic potential modulation, or a nonuniform hybridization with the substrate. In addition, it should be possible to apply the mapping to systems with an electron-electron interaction between the wire and the adjacent substrate chain. We illustrate this procedure for a substrate dispersion of the form (8), written in a mixed (k_x, y, z) representation. We can then perform the Lanczos iteration starting from the site $(k_x, y_0, z = 1)$ to obtain a

chain representation. For a metallic substrate this gives $A_n(k_x) = \epsilon_s - 2t_s \cos(k_x)$ for $n \geq 0$ and

$$B_1^2(k_x) = 3t_s^2, \quad (51a)$$

$$B_2^2(k_x) = \frac{11}{3}t_s^2, \quad (51b)$$

$$B_3^2(k_x) = \frac{125}{33}t_s^2. \quad (51c)$$

Hence, similar to the translation-invariant case, we obtain a ladder representation for the substrate by transforming back to real-space along the x -direction. A general wire-substrate hybridization can then be introduced in the form of an x -dependent hopping between the wire and the adjacent leg of the effective ladder model.

IV. EFFECTIVE NARROW LADDER MODELS

The above mapping of the wire-substrate model is exact. However, the resulting ladder representation corresponds to an anisotropic 2D system rather than a quasi-1D system because the number of legs is proportional to the number N_{imp} of single-particle states in a (yz) -slice of the system and thus generally very large. Nevertheless, we have at least two reasons to believe that quasi-1D effective systems on narrow ladders can be sufficient to accurately represent the wire-substrate system.

First, intuitively, 1D physics (such as Luttinger liquid behavior) should occur in the wire or in a region of the substrate around the wire. This corresponds to legs that are close to the wire in the ladder representation, see Fig. 1. Thus, the legs that are distant from the wire should not be essential for a qualitative description of 1D properties. Second, it can be shown [34] that the size of an effective representation for the environment of a quantum subsystem does not need to be larger than the size of the subsystem itself. In our problem, this implies that, in principle, the substrate can be represented by an effective lattice that is not larger than the wire, i.e., by a single leg. Unfortunately, in that case the effective Hamiltonian depends on the specific quantum state considered and the only known method for determining it exactly is to solve the full wire-substrate model.

Therefore, in this section, we explore the applicability of effective narrow ladder models (NLMs) with N_{leg} legs, obtained by considering only the legs closest to the wire in the ladder representation (50). The focus will be on the single-particle densities of states and the k_x -resolved single-particle spectral functions. The spectral function for the wire is defined in the momentum-space representation (17) by

$$A_w(\omega, k_x) = \sum_{\alpha} \left| \langle \alpha | d_{wk_x\sigma}^\dagger | 0 \rangle \right|^2 \delta(\omega - E_\alpha + E_0) + \sum_{\alpha} \left| \langle \alpha | d_{wk_x\sigma} | 0 \rangle \right|^2 \delta(\omega + E_\alpha - E_0), \quad (52)$$

where $|\alpha\rangle$ and E_α denote the many-body eigenstates and eigenvalues of H in its representation (50) with N_{leg} substituted for N_{imp} , while $|0\rangle$ and E_0 indicate the ground state and its energy.

In the real-space ladder representation (Sec. III C), the k_x -resolved spectral functions $A(\omega, k_x, n)$ are defined for each leg $n \geq 0$ by the same expression (52) with $f_{k_x n \sigma}^\dagger$ and $f_{k_x n \sigma}$ substituted for $d_{wk_x\sigma}^\dagger$ and $d_{wk_x\sigma}$. Obviously, $A(\omega, k_x, n = 0) = A_w(\omega, k_x)$ while $A(\omega, k_x, n \geq 1)$ relates to single-particle excitations in the substrate and the overall spectral function for the substrate $A_s(\omega, k_x)$ is obtained by averaging over all $n \geq 1$.

Similarly, in the mixed representation (k_x, y, z) (see Sec. III A), the spectral function $A_s(\omega, k_x, y, z)$ is obtained through substitution of $h_{bk_x y z \sigma}^\dagger$ and $h_{bk_x y z \sigma}$ for $d_{wk_x\sigma}^\dagger$ and $d_{wk_x\sigma}$ in the definition of $A_w(\omega, k_x)$, where $b = s$ for a metallic substrate while we average over both bands ($b = v, c$) for an insulating substrate. Here we introduced a mixed-representation fermion operator

$$h_{bk_x y z \sigma}^\dagger = \frac{1}{\sqrt{L_x}} \sum_x e^{ik_x x} c_{b\mathbf{r}\sigma}^\dagger \quad (53)$$

that creates an electron with spin σ and momentum k_x in the wire direction and coordinates (y, z) in the other directions. Hence, $A_s(\omega, k_x, y, z)$ is the k_x -resolved spectral function for a substrate chain parallel to the atomic wire at position (y, z) . Finally, the overall spectral function for the substrate $A_s(\omega, k_x)$ is obtained by averaging $A_s(\omega, k_x, y, z)$ over all coordinates y and z .

The densities of states (DOSs) in the wire ($b = w$) and the substrate ($b = s$) are

$$D_b(\omega) = \frac{1}{L_x} \sum_{k_x} A_b(\omega, k_x). \quad (54)$$

With these definitions, both DOSs are normalized, i.e., their integral over all frequencies ω equals one. Thus, we have defined the spectral functions and DOSs of the NLM (50) for any $N_{\text{leg}} \leq N_{\text{imp}}$. For $N_{\text{leg}} = N_{\text{imp}}$, we recover the spectral functions and DOSs of the full wire-substrate system. The normalized total DOS of the NLM is $D(\omega) = [D_w(\omega) + (N_{\text{leg}} - 1)D_s(\omega)]/N_{\text{leg}}$, so that the spectral weight of the wire becomes negligible compared to that of the substrate for $N_{\text{leg}} \gg 1$. In the remainder of this section, we assess the quality of the NLM approximation first for a noninteracting wire and then for a correlated wire by comparing spectral functions.

A. Noninteracting wire

For noninteracting systems [i.e., $U = 0$ in Eq. (14)], we focus on comparing spectral properties of the full system with those of the NLM with various numbers of legs N_{leg} . The electron spin will be omitted in this section as it just gives an overall factor of two. To compute spectral

properties, we used the Hamiltonians H_{k_x} in their tridiagonal Lanczos representations (32), projected onto the subspace given by the first N_{leg} Lanczos vectors, i.e., substituting $N_{\text{leg}} \leq N_{\text{imp}}$ for N_{imp} in Eq. (32). Let $\psi_{\lambda k_x}(n)$ and $\varepsilon_{\lambda k_x}$ ($\lambda = 1, \dots, N_{\text{leg}}$) denote the one-particle eigenstates and eigenvalues of these Hamiltonians. The spectral function in this chain representation is given by

$$A(\omega, k_x, n) = \sum_{\lambda=1}^{N_{\text{leg}}} |\psi_{\lambda k_x}(n)|^2 \delta(\omega - \varepsilon_{\lambda k_x}) \quad (55)$$

and can be easily calculated for any $1 \leq N_{\text{leg}} \leq N_{\text{imp}}$. As discussed above, the k_x -resolved spectral function for the wire is given by

$$A_w(\omega, k_x) = A(\omega, k_x, 0), \quad (56)$$

whereas for the substrate we have

$$A_s(\omega, k_x) = \frac{1}{N_{\text{leg}} - 1} \sum_{n=1}^{N_{\text{leg}}-1} A(\omega, k_x, n). \quad (57)$$

For insulating substrates, we can find model parameters such that some single-particle eigenenergies lie in the substrate band gap. The corresponding eigenstates are then localized on or around the wire, i.e., the density $|\psi_{\lambda k_x}(n)|^2$ remains finite on the wire sites ($n = 0$) or the neighboring substrate sites (small n) for $N_{\text{imp}} \rightarrow \infty$. These states form a band in the k_x -direction within the substrate band gap. A wave packet built from such states remains in or around the wire but can travel freely in the wire direction. Hence, the states represent a 1D electronic subsystem in the 3D wire-substrate system and will be our focus. (Other cases, such as all single-particle energies inside the valence or conduction bands, are not relevant for real wire-substrate materials.)

Figure 4 shows spectral functions and DOSs for a noninteracting wire on an insulating substrate. The wire hopping is $t_w = 3$ while the hybridization between wire and substrate is chosen to be $t_{ws} = 0.5$. (For all examples discussed in Sec. IV, we will only use a symmetric wire-substrate hybridization $t_{wc} = t_{wv}$; in the following this parameter will be denoted as t_{ws} .) The substrate parameters are $t_c = t_v = 1$ and $\epsilon_c = -\epsilon_v = 7$. The system sizes are $L_x = 256$, $L_y = 32$ and $L_z = 8$. Half-filling corresponds to the Fermi energy $\epsilon_F = 0$. These model parameters correspond to an indirect gap $\Delta_s = 2$ and a constant direct gap $\Delta(k_x) = 6$ for all k_x in the substrate single-particle spectrum in the absence of a wire, or for a vanishing wire-substrate coupling (i.e., $t_{ws} = 0$).

These gaps remain visible for a nonzero wire-substrate hybridization, as illustrated for $t_{ws} = 0.5$ in Fig. 4. The wire spectral weight is concentrated in a single band within the substrate band gap and crosses the Fermi energy $\epsilon_F \approx 0$ if the system is at or close to half-filling. This band resembles the cosine dispersion (16) of the uncoupled wire but has a small intrinsic width due to the wire-substrate hybridization t_{ws} . Only the wire band edges at

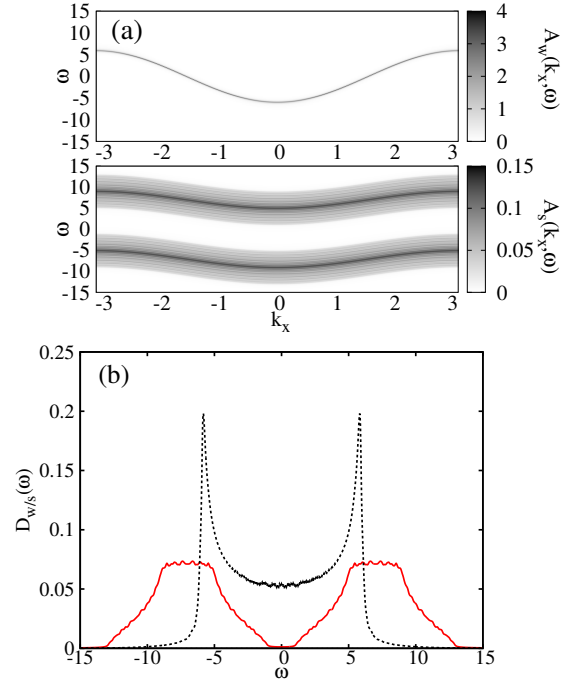


FIG. 4. (Color online) Spectral properties of a noninteracting wire on an insulating 3D substrate with $N_{\text{leg}} = N_{\text{imp}} = 513$. The other parameters are given in the text. (a) Spectral functions in the wire [$A_w(\omega, k_x)$, top] and the substrate [$A_s(\omega, k_x)$, bottom]. (b) DOS in the wire [$D_w(\omega)$, dotted black line] and in the substrate [$D_s(\omega)$, solid red line].

$k_x \approx \pm\pi$ and $k_x \approx 0$ overlap with the substrate conduction and valence bands in the spectral functions shown in Fig. 4(a). As we can see in Fig. 4(b), the DOS $D_w(\omega)$ of the wire retains the typical profile of a 1D tight-binding system with square-root singularities at the band edges close to $\pm 2t_w$. In the substrate, $D_s(\omega)$ exhibits the overall shape of a 3D tight-binding system despite the fact that the DOSs overlap over a broad energy range. This confirms that an effective quasi-1D electron system subsists in the wire despite the nonnegligible wire-substrate hybridization t_{ws} . Note that the continuous but jagged DOS curves arise from finite-size effects and a broadening of δ -peaks into Lorentzians of width $\eta = 0.1$.

For a stronger hybridization t_{ws} , we observe three bands situated symmetrically around the middle of the substrate band gap in the wire spectral functions. The distance between these bands grows with t_{ws} and for strong enough hybridization (e.g., $t_{ws} = 8$) the lower and upper bands are located below the valence band and above the conduction band, respectively. The dispersive central band is similar to the single band found at smaller t_{ws} and shown in the upper panel of Fig. 4(a). This feature can be understood in the limit of strong hybridization $\epsilon_c - \epsilon_v, t_{ws} \gg t_w \gg t_s$. In first approximation, each wire site forms a trimer with the two orbitals on its first nearest-neighbor substrate site because of their strong effective rung hoppings, see Eq. (36). The wire hopping

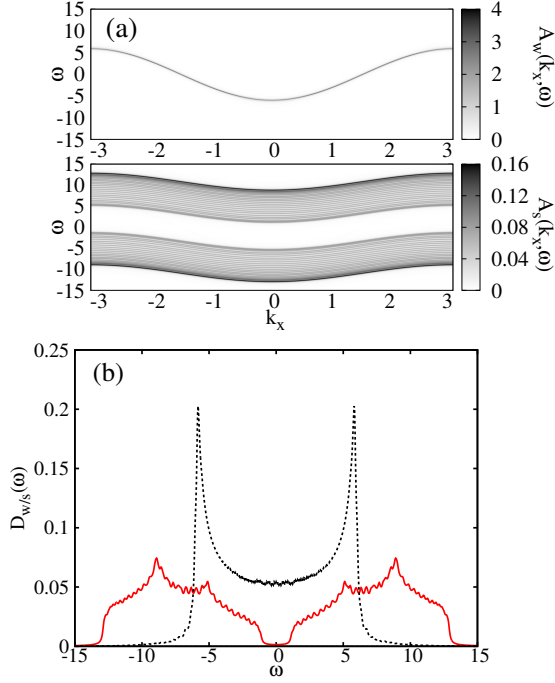


FIG. 5. (Color online) As in Fig. 4 but for an effective ladder model with $N_{\text{leg}} = 51$ legs.

t_w then leads to the formation of a strong-rung three-leg ladder made of these same sites. The single-particle eigenenergies of this system form three bands of width $\propto t_w$, which are finally slightly hybridized with the rest of the substrate by a weak effective coupling $\propto t_s$. The eigenstates of the central band that are within the substrate band gap are localized on the wire and its first nearest-neighbor substrate sites but delocalized in the wire direction. Thus they form a quasi-1D electron system on and around the wire like the eigenstates of the single band found at weaker hybridization.

The wire-substrate system can be mapped exactly to a 2D ladder-like system with $N_{\text{imp}} = 2L_y L_z + 1 = 513$ legs (see Sec. III). Here, we examine NLMs with $N_{\text{leg}} < N_{\text{imp}}$. Figures 5 and 6 show results for the spectral functions and the DOS for $N_{\text{leg}} = 51$ and $N_{\text{leg}} = 3$, respectively. The other parameters are the same as for the case of the full system shown in Fig. 4. Overall, we find that the NLM can describe the full system correctly if two conditions are fulfilled. First, the number of legs must be an odd number. This condition can be easily interpreted: the NLM must include an even number of legs representing the substrate (besides the leg representing the wire) to keep an equal number of degrees of freedom for the valence and conduction bands. Accordingly, an NLM must have at least three legs to describe a wire on an insulating substrate. Second, the number of substrate legs must be large enough to represent the energy range of the valence and conduction bands correctly, e.g., the band gap. This condition can be achieved, however, using many fewer legs than in the full system, i.e., for $N_{\text{leg}} \ll N_{\text{imp}}$.

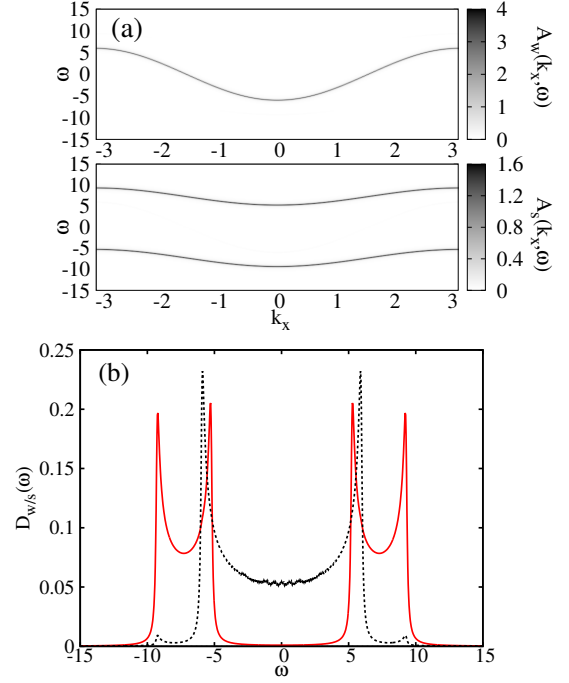


FIG. 6. (Color online) As in Fig. 4 but for a narrow ladder model with $N_{\text{leg}} = 3$ legs.

For instance, the energy range of the substrate bands is already well represented for $N_{\text{leg}} = 51 \ll N_{\text{imp}} = 513$ in Fig. 5, although the spectral weight deviates visibly from that of the full system shown in Fig. 4. In contrast, Fig. 6 shows that the spectral functions and DOS of the substrate are poorly represented by the NLM with $N_{\text{leg}} = 3$ as the spectral weight remains concentrated in two narrow bands. In particular, the effective substrate band gap is $\Delta_s(N_{\text{leg}} = 3) \approx 10$ and thus five times larger than the true gap $\Delta_s = 2$ while the DOS exhibits van Hove singularities typical of two-leg ladders.

Nevertheless, the wire spectral properties in the NLM with $N_{\text{leg}} \geq 3$ agree quantitatively with those of the 3D wire-substrate system close to the middle of the spectrum ($\omega \approx 0$). Comparing with Fig. 4(b) we see that the wire DOS in Fig. 5(b) is reproduced correctly for $N_{\text{leg}} = 51$, while for $N_{\text{leg}} = 3$ [Fig. 6(b)] it is substantially modified only where it overlaps with the substrate DOS ($|\omega| \gtrsim 4$). Therefore, our analysis suggests that a three-leg NLM close to half-filling can be used to describe the low-energy properties of a weakly interacting wire on an insulating substrate, at least qualitatively, as the degrees of freedom close to the Fermi energy ($\epsilon_F \approx 0$) are correctly represented. For instance, one could study the stability of Luttinger liquid features in a 1D conductor deposited on an insulating substrate beyond the minimal models used previously [14–16]. However, for strong interactions or for a quantitative description of the 3D wire-substrate system by an effective NLM, we expect wider ladders and an analysis of the convergence with N_{leg} to be necessary. Still, our results for noninteracting wires suggest

that the required N_{leg} can be significantly smaller than the substrate size N_{imp} , making the NLMs amenable to standard methods for quasi-1D correlated systems. The same holds true for interacting systems, as demonstrated in Sec. IV B. A detailed study of a correlated wire with a Hubbard interaction can be found in [30].

Finally, for a metallic substrate, we unsurprisingly find all single-electron eigenstates to be delocalized over the entire wire-substrate system. (Of course there exist localized single-particle states in the wire for energies above or below the metallic band, but these states are not relevant for real materials.) Therefore, we do not observe any 1D features in a noninteracting wire coupled to a metallic substrate, but this could be modified by interactions. More decisively, we find that the spectral properties at the Fermi energy vary strongly with the number of legs in the NLM (50) even when N_{leg} is as large as 51. Therefore, we conclude that the full wire-substrate system cannot be represented even qualitatively by a quasi-1D NLM if the substrate is metallic.

B. Interacting wire

Having established the usefulness of NLMs in the noninteracting case, we briefly consider a correlated wire with a repulsive Hubbard interaction $U \geq 0$ [cf. Eq. (14)]. A detailed investigation of this problem, including the Mott-insulating and Luttinger-liquid phases, can be found in [30] where we also discuss the physics of the 1D Hubbard model. Here, we compare spectral functions for the 3D wire-substrate problem to those of the NLM (50) with $N_{\text{leg}} = 3$. The onsite potential in the wire is $\epsilon_w = -U/2$, so that the Hubbard bands are situated symmetrically around the middle of the substrate band gap. The other parameters are taken to be the same as in Figs. 4–6. We focus on a single set of parameters in the metallic (Luttinger liquid) phase that exists away from half-filling. The interacting problem is solved by the continuous-time interaction expansion (CT-INT) quantum Monte Carlo method [28], which can be used to simulate the 3D wire-substrate system and NLMs with the same numerical effort. For details see [30].

At half-filling, the full wire-substrate model contains $N_p = N_{\text{imp}}L_x$ electrons, whereas $N_p = N_{\text{leg}}L_x$ for the NLM. If the system is doped away from half-filling with a finite bulk doping $y \in (-1, 1)$ [i.e., $N_p = (1+y)N_{\text{imp}}L_x$ electrons in the full wire-substrate system or $N_p = (1+y)N_{\text{leg}}L_x$ in the NLM], the chemical potential will lie in one of the substrate bands. This situation corresponds to a metallic substrate, which is neither relevant for atomic wires deposited on semiconducting substrates nor expected to be well represented by an NLM. A more interesting and relevant case is that of a finite wire doping $y_w \in (-1, 1)$ ($N_p = N_{\text{imp}}L_x + y_wL_x$ for the full wire-substrate model, or $N_p = N_{\text{leg}}L_x + y_wL_x$ for the NLM) but a vanishing bulk doping [$y \approx 0$ and $N_p/(N_{\text{imp}}L_x) \approx 1$]. In the latter, our wire-substrate model can describe a

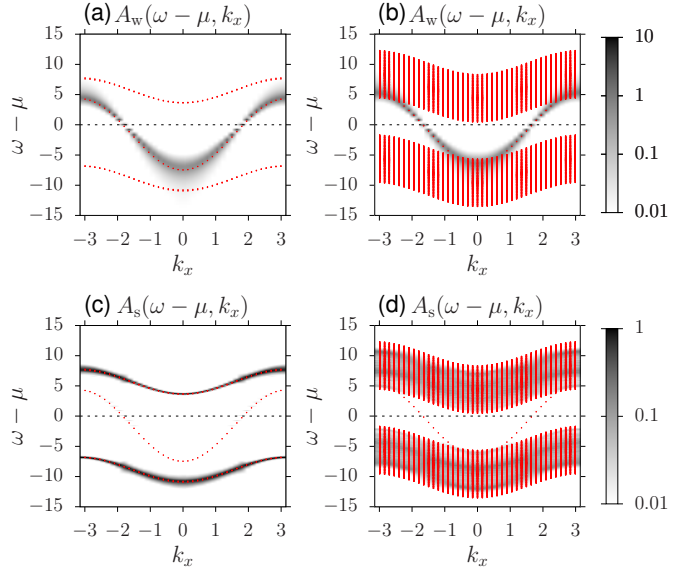


FIG. 7. (Color online) Spectral functions calculated for an interacting wire ($U = 4$) as obtained from CT-INT QMC simulations with $\beta = 15$. The chemical potential was tuned to obtain a wire doping $y_w \approx 12.5\%$. Top: wire spectral function $A_w(\omega, k_x)$ for (a) the three-leg NLM and (b) the 3D wire-substrate model. Bottom: (c) substrate spectral function $A_s(\omega, k_x)$ for the three-leg NLM, (d) substrate spectral function $A_s(\omega, k_x)$ of the full model averaged over the chains at the minimal and the maximal distance from the wire. In all cases, $L_x = 42$, and for the 3D substrate lattice $L_y = 42$ and $L_z = 10$. All other parameters as in Figs. 4–6. Red symbols illustrate the noninteracting energy levels.

quasi-1D conductor embedded in an insulating 3D bulk system, as relevant for metallic wires on semiconducting substrates. Besides In/Si(111) [9] above its critical temperature as well as the Au/Ge(100) [11, 35–38] and Bi/InSb(100) [12] systems mentioned in Sec. I, Pt/Ge(100) [39, 40], Pb/Si(557) [41], and dysprosium silicide nanowires on Si(001) surfaces [42] are also known to be metallic.

We calculated the finite-temperature analogs of the single-particle spectral functions $A_w(\omega, k_x)$, $A(\omega, k_x, n)$, and $A_s(\omega, k_x, y, z)$ defined at the beginning of Sec. IV. For example, the wire spectral function is given by

$$A_w(\omega, k_x) = \frac{1}{Z} \sum_{ij} |\langle i | d_{wk_x\sigma} | j \rangle|^2 (e^{-\beta E_i} + e^{-\beta E_j}) \times \delta(\Delta_{ji} - \omega) \quad (58)$$

and can be obtained from the single-particle Green function $G(k, \tau) = \langle d_{wk_x\sigma}^\dagger(\tau) d_{wk_x\sigma}(0) \rangle$ by analytic continuation [43]. In Eq. (58), Z is the grand-canonical partition function, $|i\rangle$ is an eigenstate with energy E_i , and $\Delta_{ji} = E_j - E_i$. Similarly, we can obtain $A(\omega, k_x, n)$ in the NLM and $A_s(\omega, k_x, y, z)$ for specific chains in the substrate of the 3D wire-substrate model. Because a full substrate average is expensive with the CT-INT method, substrate

properties were averaged over the chains at the minimal ($y = y_0, z = 1$) and maximal ($y = y_0 + L_y/2, z = L_z$) distance from the wire.

For sufficiently weak coupling U , we find that a metallic wire is realized in both the 3D wire-substrate model and in the NLM at low wire doping. As an example, Fig. 7 compares the spectral functions $A_w(\omega, k_x)$ and $A_s(\omega, k_x, y = y_0, z = 1)$ of the 3D wire-substrate model with the spectral functions $A_w(\omega, k_x)$ and $A_s(\omega, k_x)$ of the three-leg NLM at $U = 4$. The chemical potential was set to $\mu = 1.58$ for the NLM and to $\mu = 0.60$ for the full model, corresponding to a total doping of 5.25(1) electrons (or $y_w \approx 12.5\%$ for $L_x = 42$). A comparison of Figs. 7(a) and (b) reveals that the wire spectral functions of the two models agree close to the Fermi energy, and that there exist gapless excitations predominantly localized in the wire. In contrast, the substrate spectral functions in Figs. 7(c) and (d) differ significantly, as already observed for the noninteracting case. Nevertheless, both models exhibit a vanishingly small weight at the Fermi energy.

These QMC results confirm that—similar to the noninteracting case—the low-energy excitations of a metallic interacting wire in the 3D wire-substrate model are well represented, at least qualitatively, by the three-leg NLM for moderate couplings U . For strong interactions, however, the low-energy excitations can be delocalized in the substrate and the NLM approximation becomes less accurate. This regime is discussed in detail in [30].

V. CONCLUSIONS

We introduced lattice models for correlated atomic wires on noninteracting metallic or insulating substrates, and showed that they can be mapped exactly onto ladder-like 2D lattices. The first leg corresponds to the atomic wire, while the other legs represent successive shells of

substrate sites with increasing distance from the wire. We investigated the approximation of narrow ladder models that take only a few shells around the wire into account. Our results suggest that the low-energy physics of (weakly-interacting) wires on insulating substrates can be described by ladder models with three or more legs. These models can be studied with well-established methods for 1D correlated systems such as the DMRG [17–20] or field-theoretical techniques (e.g., bosonization and the renormalization group) [1, 6, 21–23]. We believe that the approach developed here can shed new light on the quasi-1D physics and correlation effects to be found in atomic wires deposited on semiconducting substrates. As a first application, we investigate Mott and Luttinger liquid phases of a Hubbard-type wire on an insulating substrate using DMRG and QMC methods in [30].

In the future, we plan to apply this approach to real metallic wire-substrate systems. The wire-substrate model defined in Sec. II can easily be generalized to achieve a more realistic description of specific experiments. In particular, one can use first-principles band structures and hybridizations [44–47] for the noninteracting part of the Hamiltonian. However, determining the interaction parameters from first-principles simulations remains an open problem [48].

ACKNOWLEDGMENTS

This work was supported by the German Research Foundation (DFG) through SFB 1170 ToCoTronics and the Research Unit *Metallic nanowires on the atomic scale: Electronic and vibrational coupling in real world systems* (FOR 1700, grant No. JE 261/1-1). The authors gratefully acknowledge the computing time granted by the John von Neumann Institute for Computing (NIC) and provided on the supercomputer JURECA [49] at the Jülich Supercomputing Centre.

-
- ¹ J. Sólyom, *Advances in Physics* **28**, 201 (1979).
 - ² H. Kiess (ed.), *Conjugated Conducting Polymers* (Springer, Berlin, 1992).
 - ³ G. Grüner, *Density Waves in Solids* (Perseus Publishing, Cambridge, 2000).
 - ⁴ D. Baeriswyl and L. Degiorgi (Eds.), *Strong Interactions in Low Dimensions* (Kluwer Academic Publishers, Dordrecht, 2004).
 - ⁵ F. H. L. Eßler, H. Frahm, F. Göhmann, A. Klümper and V. E. Korepin, *The One-Dimensional Hubbard Model* (Cambridge University Press, Cambridge, 2005).
 - ⁶ T. Giamarchi, *Quantum Physics in One Dimension* (Oxford University Press, Oxford, 2007).
 - ⁷ M. Springborg and Y. Dong, *Metallic Chains / Chains of Metals* (Elsevier, Amsterdam, 2007).
 - ⁸ N. Oncel, *J. Phys.: Condens. Matter* **20**, 393001 (2008).
 - ⁹ P. C. Snijders and H. H. Weitering, *Rev. Mod. Phys.* **82**, 307 (2010).
 - ¹⁰ E. Jeckelmann, S. Sanna, W. G. Schmidt, E. Speiser, and N. Esser, *Phys. Rev. B* **93**, 241407 (2016).
 - ¹¹ C. Blumenstein, J. Schäfer, S. Mietke, S. Meyer, A. Dollinger, M. Lochner, X. Y. Cui, L. Patthey, R. Matzdorf, and R. Claessen, *Nature Physics* **7**, 776 (2011).
 - ¹² Y. Ohtsubo, J. Kishi, K. Hagiwara, P. Le Fèvre, F. Bertran, A. Taleb-Ibrahimi, H. Yamane, S. Ideta, M. Matsunami, K. Tanaka, and S. Kimura, *Phys. Rev. Lett.* **115**, 256404 (2015).
 - ¹³ J. Aulbach, J. Schäfer, S. C. Erwin, S. Meyer, C. Lohö, J. Settlein, and R. Claessen, *Phys. Rev. Lett.* **111**, 137203 (2013).
 - ¹⁴ I. K. Dash and A. J. Fisher, *J. Phys.: Condens. Matter* **13**, 5035 (2001).
 - ¹⁵ I. K. Dash and A. J. Fisher, e-print arXiv:cond-mat/0210611v1.
 - ¹⁶ A. Abdelwahab, E. Jeckelmann, and M. Hohenadler, *Phys. Rev. B* **91**, 155119 (2015).

- ¹⁷ S. R. White, Phys. Rev. Lett. **69**, 2863 (1992).
- ¹⁸ S. R. White, Phys. Rev. B **48**, 10345 (1993).
- ¹⁹ U. Schollwöck, Rev. Mod. Phys. **77**, 259 (2005).
- ²⁰ E. Jeckelmann, in *Computational Many Particle Physics* (Lecture Notes in Physics **739**), edited by H. Fehske, R. Schneider, and A. Weiße (Springer Verlag, Berlin, Heidelberg, 2008), p. 597.
- ²¹ K. Schönhammer, *Luttinger liquids: the basic concepts*, Chap. 4 of Ref. [4].
- ²² A. O. Gogolin, A. A. Nersesyan, A. M. Tsvelik, *Bosonization and Strongly Correlated Systems*, Cambridge University Press 1998.
- ²³ A. M. Tsvelik, *Quantum Field Theory in Condensed Matter Physics*, Cambridge University Press 2003.
- ²⁴ T. Shirakawa and S. Yunoki, Phys. Rev. B **90**, 195109 (2014).
- ²⁵ A. Allerdtd, C. A. Büsser, G. B. Martins, and A. E. Feiguin, Phys. Rev. B **91**, 085101 (2015).
- ²⁶ K. G. Wilson, Rev. Mod. Phys. **47**, 773 (1975).
- ²⁷ D. C. Mattis in J. Bernasconi and T. Schneider (eds.), *Physics in One Dimension* (Springer, Berlin, 1981).
- ²⁸ A. N. Rubtsov, V. V. Savkin, and A. I. Lichtenstein, Phys. Rev. B **72**, 035122 (2005).
- ²⁹ E. Gull, A. J. Millis, A. I. Lichtenstein, A. N. Rubtsov, M. Troyer, and P. Werner, Rev. Mod. Phys. **83**, 349 (2011).
- ³⁰ Second paper of this series: A. Abdelwahab, E. Jeckelmann, and M. Hohenadler, e-print arXiv:1704.07359.
- ³¹ P. A. Ignatiev, N. N. Negulyaev, L. Niebergall, H. Hashemi, W. Hergert, and V. S. Stepanyuk, Phys. Status Solidi B **247**, 2537 (2010).
- ³² G. D. Mahan, *Many-Particle Physics* (Kluwer Academic, New York, 2000).
- ³³ D. Ruhl and F. Gebhard, Phys. Rev. B **83**, 035120 (2011).
- ³⁴ G. Knizia and G. K.-L. Chan, Phys. Rev. Lett. **109**, 186404 (2012).
- ³⁵ C. Blumenstein, J. Schäfer, S. Mietke, S. Meyer, A. Dollinger, M. Lochner, X. Y. Cui, L. Patthey, R. Matzdorf, and R. Claessen, Nature Physics **8**, 174 (2012).
- ³⁶ K. Nakatsuji and F. Komori, Nature Physics **8**, 174 (2012).
- ³⁷ J. Park, K. Nakatsuji, T.-H. Kim, S. K. Song, F. Komori, and H. W. Yeom, Phys. Rev. B **90**, 165410 (2014).
- ³⁸ N. de Jong, R. Heimbuch, S. Eliens, S. Smit, E. Frantzeskakis, J.-S. Caux, H. J. W. Zandvliet, M. S. Golden, Phys. Rev. B **93**, 235444 (2016).
- ³⁹ K. Yaji, I. Mochizuki, S. Kim, Y. Takeichi, A. Harasawa, Y. Ohtsubo, P. Le Fèvre, F. Bertran, A. Taleb-Ibrahimi, A. Kakizaki, and F. Komori, Phys. Rev. B **87**, 241413 (2013).
- ⁴⁰ K. Yaji, S. Kim, I. Mochizuki, Y. Takeichi, Y. Ohtsubo, P. Le Fèvre, F. Bertran, A. Taleb-Ibrahimi, S. Shin, and F. Komori, J. Phys.: Condens. Matter **28**, 284001 (2016).
- ⁴¹ C. Tegenkamp, Z. Kallassy, H. Pfnür, H.-L. Günter, V. Zielasek, and M. Henzler, Phys. Rev. Lett. **95**, 176804 (2005).
- ⁴² M. Wanke, K. Löser, G. Pruskil, D. V. Vyalikh, S. L. Molodtsov, S. Danzenbächer, C. Laubschat, and M. Dähne, Phys. Rev. B **83**, 205417 (2011).
- ⁴³ K. S. D. Beach, arXiv:cond-mat/0403055 (2004).
- ⁴⁴ L. Cano-Cortés, A. Dolfen, J. Merino, J. Behler, B. Delley, K. Reuter, and E. Koch, Eur. Phys. J. B **56**, 173 (2007).
- ⁴⁵ K. Nakamura, Y. Yoshimoto, T. Kosugi, R. Arita, and M. Imada, J. Phys. Soc. Jpn. **78**, 083710 (2009).
- ⁴⁶ H. C. Kandpal, I. Opahle, Y.-Z. Zhang, H. O. Jeschke, and R. Valenti, Phys. Rev. Lett. **103**, 067004 (2009).
- ⁴⁷ M. Tsuchiizu, Y. Omori, Y. Suzumura, M.-L. Bonnet, and V. Robert, J. Chem. Phys. **136**, 044519 (2012).
- ⁴⁸ R. M. Lee and N. D. Drummond, Phys. Rev. B **83**, 245114 (2011).
- ⁴⁹ Jülich Supercomputing Centre (2016), JURECA: General-purpose supercomputer at Jülich Supercomputing Centre, Journal of large-scale research facilities, **2**, A62. <http://dx.doi.org/10.17815/jlsrf-2-121>